ACS APPLIED MATERIALS & INTERFACES

Research Article

Cite This: ACS Appl. Mater. Interfaces 2019, 11, 35221−35227

www.acsami.org

Delamination Mechanics of Carbon Nanotube Micropillars

Josef Brown,[†] Taher Hajilounezhad,[†] Nicholas T. Dee,[‡] Sanha Kim,[‡] A. John Hart,[‡] and Matthew R. Maschmann*[,†]

[†]Department of Mechanical and Aerospace Engineering, University of Missouri, Columbia, Missouri 65201, United States

[‡]Department of Mechanical Engineering, Massachusetts Institute of Technology, Cambridge, Massachusetts 02139, United States

Supporting Information

ABSTRACT: The adhesion of carbon nanotube (CNT) forests to their growth substrate is a critical concern for many applications. Here, we measured the delamination force of CNT forest micropillars using in situ scanning electron microscopy (SEM) tensile testing. A flat tip with epoxy adhesive first established contact with the top surface of freestanding CNT pillars and then pulled the pillars in displacement-controlled tension until delamination was observed. An average delamination stress of 6.1 MPa was measured, based on the full pillar cross-sectional area, and detachment was observed to occur between catalyst particles and the growth substrate. Finite element simulations of CNT forest delamination show that force and strain are heterogeneously distributed among CNTs during tensile loading and that CNTs progressively lose adhesion with increased displacement. Based on combined experiments and simulations, an adhesion strength of approximately 350 MPa was estimated between each CNT and the substrate. These findings provide important insight into CNT applications such as thermal interfaces, mechanical sensors, and structural composites while also suggesting a potential upper limit of tensile forces allowed during CNT forest synthesis.

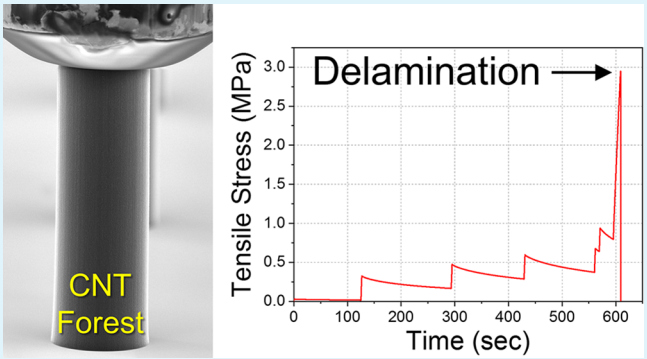

KEYWORDS: *delamination, adhesion, carbon nanotubes, simulation, in situ scanning electron microscopy*

1. INTRODUCTION

CNT forests are populations of CNTs that self-assemble into vertically oriented films during synthesis. The chemical vapor deposition (CVD) processing of CNT forests is amenable to scale-up,[1] making CNT forests appealing for applications including thermal interfaces,[2,3] mechanical sensing,[4,5] electrical vias and interconnects,[6,7] composite materials,[8−10] and dry adhesives.[11,12] While these applications rely on the robust adhesion of CNTs to their growth substrate, anecdotally, CNT forest adhesion to a growth substrate is often considered to be weak. Characterizing and understanding the mechanisms of CNT−substrate interface adhesion is an important step toward realizing CNT forest-based applications and devices.

Various methods have been used to study the adhesion of CNT forests to substrates including scratch testing,[13,14] peel-off testing,[15] indentation,[16] sonication,[17] and removal by AFM tip.[18] The diversity of test methods leads to variable mechanical loading conditions and different delamination metrics. The direct CNT forest removal from SiC wire substrates was achieved using an adhesive tape peel-off method. The average delamination stress measured by this method was 0.28 MPa for as-grown CNT forests and 0.5 MPa after annealing the CNT forest after growth at 950 °C in Ar.[15] In a separate study, CNT forest buckling induced by indentation produced localized CNT delamination in and around the indented area, with an estimated delamination stress of 0.4−0.8 MPa.[16] Both of these tests applied mixed loading conditions consisting of combined axial tension and shear. Direct tensile loading supplied by an AFM tip to large-diameter CNTs measured an adhesion force of 2−8 μN/CNT for CNTs with outer diameters ranging from 70−110 nm.[18] Scratch testing is an alternative adhesion testing methodology that measures the lateral force obtained by translating a tip through a CNT forest while the tip retains contact with the growth substrate. After subtracting the background frictional load provided by the substrate itself, the resulting energy is determined by integrating the measured lateral force across a given scratch length. This energy is attributed to debonding CNTs from the substrate. With this technique, a delamination energy of 3 pJ/CNT was found when using a copper substrate and 0.6 pJ/CNT on a silicon substrate.[13] A similar scratch test measured the delamination energy of 13−44 pJ/CNT for CNT forests synthesized on stainless steel.[14] While scratch test results are relatively straightforward to obtain, the contributions of CNT forest deformation and friction between CNTs and the substrate to the energy measurement are not apparent

Received: June 7, 2019
Accepted: September 3, 2019
Published: September 3, 2019

DOI: 10.1021/acsami.9b09979
ACS Appl. Mater. Interfaces 2019, 11, 35221−35227

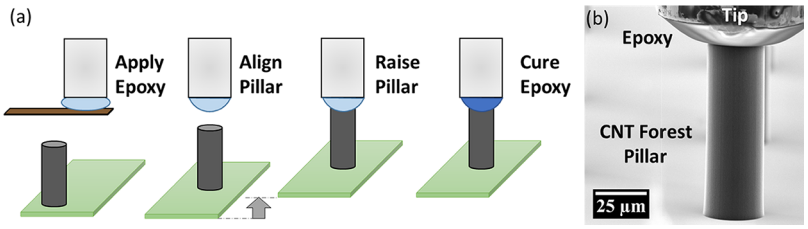

Figure 1. Adhesion of a CNT forest micropillar to an epoxy-coated test tip. (a) Schematic of epoxy application, pillar alignment, pillar insertion into epoxy, and epoxy curing. (b) SEM image showing the application of epoxy to the top surface of a cylindrical CNT forest micropillar.

and are not considered in reported results. Contact adhesion experiments in which the free ends of CNT forests are in contact with an external surface, may also provide insight into CNT forest delamination strength. These tests may be considered a lower bound of delamination strength because CNTs are not debonded from their growth substrate during the test. Single-walled CNT (SWNT) forests whose free tips are adhered to glass achieved an adhesion strength of 0.29 MPa between the CNTs and the glass in the normal direction[19] and 1.0 MPa in shear.[20] CNT pillar contact adhesion to a sapphire indenter tip produced an adhesion strength of 26 kPa after a compressive preload of 80 kPa.[21] Qualitative CNT forest adhesion measurements have also been reported. In these tests, substrate-adhered CNT forests were sonicated in a buffer solution, and adhesion strength was judged by the fraction of CNTs that remained on the substrate after sonication.[17] Results from these tests demonstrated that microwave exposure of CNT forests after synthesis improved substrate adhesion by subsurface diffusion of Ni catalyst particles into a 20 nm Ti support layer.[17] To further obscure the interpretation of the results obtained by these methods, it is worth noting that the catalyst, catalyst support layers, and synthesis conditions were different among all studies. It is also unclear if the CNTs were grown from the base-growth or tip-growth mechanism, obscuring the nature of the CNT−catalyst−substrate interfaces.

Postsynthesis processing of CNT forests to promote forest delamination has been reported using a variety of techniques. Direct CNT forest transfer from a growth substrate to a new host substrate consisting of polymer, functionalized SiO_2, or soft metallic foils, has been reported extensively.[22−26] In these transfer processes, the new host substrate was placed in contact with the free surface of a CNT forest in the presence of heat and/or compression. Adhesion between the free ends of the CNT forest and the new host substrate exceeded that provided by the growth substrate, resulting in a direct transfer process. In another process, CNT forest substrates were dipped into heated water. The water imparts a thermocapillary force that was sufficient to delaminate the forest from its substrate.[27] Gas-phase oxidation achieved by introduction of CO_2,[28] water vapor,[26,29] or oxygen[30] immediately after CNT synthesis has also been used to weaken the CNT forest adhesion to their growth substrates. Finally, the drawing and spinning of CNT yarns[31] from a CNT forest selectively delaminate CNT forests from their growth substrate to form a continuous fiber. Unfortunately, to date, these processes have not been instrumented to provide quantitative estimates of CNT adhesion strength.

Here, we demonstrate the use of an instrumented in situ SEM mechanical test frame to apply uniaxial tension to CNT forest micropillars for straightforward mechanical interpretation. Epoxy adhesive was first applied to the top surface of the micropillars using a flat tip, and then uniaxial tension was applied once the epoxy had cured. Previous in situ SEM mechanical tests have compressed CNT forests[19,32] and CNT forest micropillars[20,33−36] using a flat compression platen for uniaxial compression, but to the best of our knowledge, this is the first report of tensile loading for pristine CNT forests. SEM examination of the substrate delamination region and the delaminated surface of CNT forests provide insight into the detachment mechanisms. The delamination process was also studied using a finite element simulation to first synthesize CNT forests with similar characteristics as those examined experimentally and then delaminate those forests from the substrate. For clarity of terminology, we will define CNT forest delamination stress as the force required to remove a monolithic forest structure from the growth substrate divided by its apparent cross-sectional area, while CNT adhesion strength is defined as the stress required to remove a single CNT from the growth substrate.

2. EXPERIMENTAL SECTION

The CNT forest pillars were synthesized on (100) silicon wafers coated with 300 nm of thermally grown SiO_2 by patterning an Fe/Al_2O_3-supported catalyst layer by lift-off photolithography. The supported catalyst layer, 10 nm of Al_2O_3 and 1 nm of Fe, was sequentially deposited by electron beam evaporation. The patterned substrate was placed in a quartz tube furnace for the CNT growth. A catalyst preconditioning phase begins by flowing 100/400 sccm of He/H_2 while ramping the furnace to 775 °C over 10 min. Holding at 775 °C, 100 sccm of C_2H_4 is added to the He/H_2 stream for 3 min, proceeded by 7 more min without the C_2H_4. The catalyst film is then annealed at 775 °C under the same He/H_2 flow for 10 min after which the gas flow is changed to 400/100/100 sccm of $He/H_2/C_2H_4$ at 775 °C for CNT nucleation and growth for approximately 30 s to produce 100 μm tall CNT pillars. The C_2H_4 flow was extinguished to end growth, and the furnace was allowed to cool to 100 °C. A purge of 1000 sccm of He was maintained for 5 min before the samples were retrieved. Characterization of CNT forests produced by this process[37] has determined that this process generates multiwalled CNTs with an average diameter of 11 nm and a CNT areal density of 5×10^{10} CNT/cm^2. The log−normal diameter distribution may be found in the Supporting Information. Based on previous in operando TEM observations, the CNTs nucleate and grow via the base-growth mechanism, whereby the catalyst resides at the substrate surface for the duration of CNT growth.[37,38] Further, the catalyst preconditioning process has been shown to fully reduce the Fe catalyst to Fe^0 prior to CNT forest synthesis, leading to increased catalytic activity.[39]

An in situ SEM mechanical test frame (MicroTesting Solutions) was used to perform all uniaxial delamination tests, as shown schematically in Figure 1. A 100 μm diameter cylindrical sapphire tip was used as a platen to interface with the free (top) surface of the CNT forest pillars. The CNT micropillar substrate was placed on a piezoelectric stage having 3 translational degrees of freedom. Just prior to evacuating the SEM (FEI Quanta), a small quantity of 3 M epoxy (08107) was applied to the free end of the cylindrical test tip by pressing a thin film of the epoxy to the tip, and the SEM chamber was

DOI: 10.1021/acsami.9b09979
ACS Appl. Mater. Interfaces 2019, 11, 35221−35227

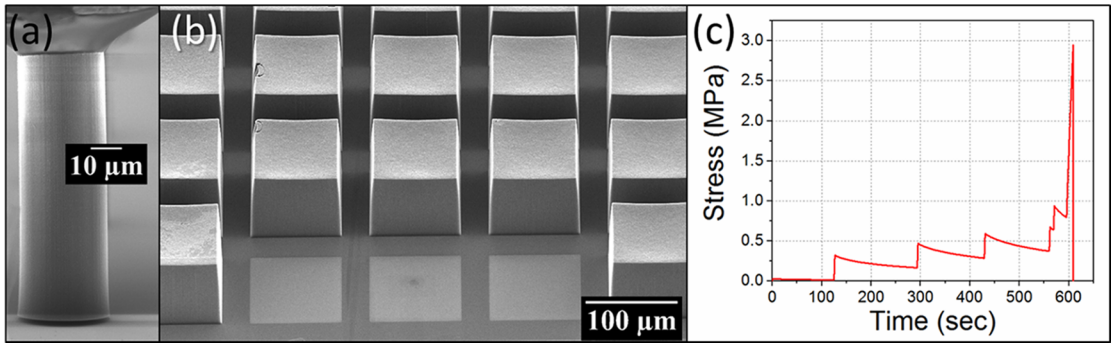

Figure 2. SEM images of (a) a delaminated CNT forest micropillar (30 μm diameter) and (b) a host silicon growth substrate with three delaminated CNT pillars (100 × 100 μm cross section). (c) Tensile stress (defined as load divided by pillar cross-sectional area) was applied stepwise, with a maximum delamination stress of 3 MPa. Note that stress relaxation occurred between incremental stepwise displacements.

evacuated. The epoxy was retained on the tip by surface tension. During the approximately 2−3 min required to attain an appropriate SEM chamber pressure for imaging, the tip with epoxy was positioned to a working distance of 100 μm above the sample. Upon attaining the appropriate vacuum pressure to enable SEM imaging, the test frame sample stage was positioned under the epoxy bulb. A CNT pillar was positioned under the tip and then gently raised into contact with the epoxy by using SEM imaging. Vertical travel of the sample was ceased after the free tips of the CNT forest were embedded approximately 1−2 μm into the epoxy. The epoxy accepted the CNT free ends without excessive wicking away from the contact area and without imposing unintended surface tension forces at the top surface of the pillar (judged by the lack of deformation of the CNT forest in the vicinity of the contact). An SEM image of a 30 μm diameter CNT forest micropillar in contact with the epoxy tip is shown in Figure 1b. It was experimentally determined that the epoxy had a working time of less than 10 min before achieving a viscosity that was too large to freely accommodate the CNT forest. After positioning of the tip onto the micropillar, the epoxy was allowed to cure in vacuum within the SEM, with the electron beam off, for a duration of 3 h or greater.

Uniaxial tensile displacement was applied to the top surface of CNT forests pillars by moving the sample stage away from the sapphire tip using the piezoelectric stage motor. Translating the substrate rather than the tip enabled a rapid and "on the fly" application of displacement throughout the test, rather than a prescribed computer-controlled displacement rate. The tensile force was measured using a 50 gram load cell located in series with the indenter tip. The application of displacement was applied stepwise to allow SEM images to be acquired between displacement increments. For these tests, discrete displacement steps of between 5−20 nm were implemented. The cured epoxy was viscoelastic such that stress and strain were relieved between applications of displacement steps. The viscoelastic compliance of the epoxy complicated the measurement of a true displacement of the CNT tips relative to the substrate; however, the force measured by the load cell accurately represented the load transmitted to the CNT forest.

3. RESULTS AND DISCUSSION

Figure 2a shows an SEM image of a delaminated CNT micropillar after tensile loading. After CNT forest delamination, the lithographically defined catalyst pads of three delaminated pillars were recognizable, as seen in Figure 2b. The stress versus time plot for a representative delamination experiment, shown in Figure 2c, readily shows the step increases in tensile force due to displacement steps, followed by a gradual viscoelastic recovery. The rate of viscoelastic recovery increased in proportion to the applied tensile load. Near the end of the test, tensile displacement was rapidly applied at a constant rate to counteract viscoelastic relaxation of the epoxy, as reflected by the nearly linear increase in tensile force with time. The tensile stress increased linearly until a peak at approximately 3 MPa, followed by an abrupt drop, as observed in Figure 2c. The rapid drop to a neutral stress indicates a rapid delamination of the CNT pillar. The peak stress achieved during the test represents the delamination stress of the CNT pillar from the substrate.

CNT forest pillars with square and circular cross sections with width or diameter of 30 and 100 μm were examined. Delamination stresses of 3.0, 7.9, 14.2, 4.0, and 1.4 MPa were measured (based on the pillar cross-sectional area). These tests provide a mean value of 6.1 MPa with a standard deviation of 5.1 MPa. The large standard deviation may result from a limited data acquisition rate (10 Hz) relative to the speed of delamination; sample-to-sample variation in CNT diameter, morphology, or areal density between pillars; or undesired prestrain imparted by the slightly tapered CNT forest pillar profile (see Figure 2b). Large sample-to-sample variation has also been observed in alternative methods.[15]

The delamination region on the growth substrate (Figure 3a) exhibits small dark pits with diameters on the order of 10

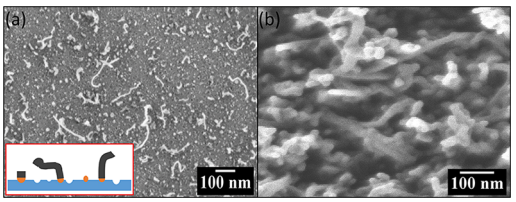

Figure 3. SEM micrographs showing (a) the substrate region in which CNT forest micropillars were delaminated from their growth substrate and (b) the CNT forest delamination surface showing closed CNT ends.

nm, suggesting that catalyst nanoparticles were lifted from the growth substrate during CNT forest removal and that the delamination mechanism occurred at the interface between catalyst particles and the substrate rather than that between the CNTs and catalyst particles. To further support this claim, we observe that the delaminated surfaces of the CNTs are closed, as shown in Figure 3b. Also present in the delaminated region are numerous short (<1 μm) CNTs. We believe that these remaining CNTs were sufficiently short that they lacked entanglement within the bulk forest. As a result, these CNTs experienced either no tensile force, or the tensile force was sufficient to overcome the van der Waals forces bonding these CNTs to other CNTs within the forest. Previous in situ SAXS measurements showed that the number density of CNTs

DOI: 10.1021/acsami.9b09979
ACS Appl. Mater. Interfaces 2019, 11, 35221−35227

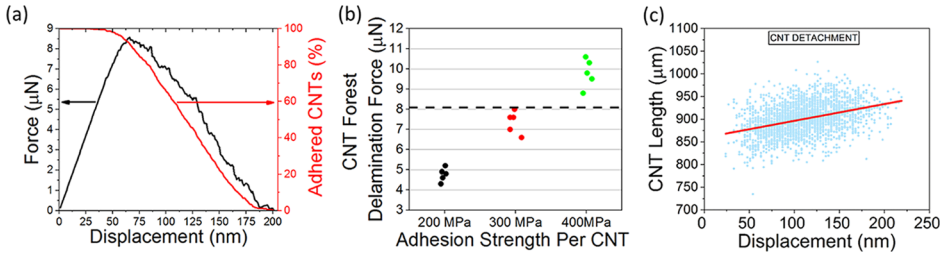

Figure 4. (a) The simulated tensile load and percentage of adhered CNTs as a function of vertical displacement. (b) The simulated CNT forest delamination force for five representative CNT forests vs CNT adhesion strength. An average delamination force of 12.2 nN per CNT was observed experimentally, corresponding to a cumulative delamination force of 8.17 μN in the simulations (with 670 CNTs), denoted by the dashed horizontal line. (c) The length of each delaminated CNT was plotted as a function of the tensile displacement at which the CNT detached. A linear trend line indicates that shorter CNTs delaminate at early stages of tensile loading. All simulations used a CNT−CNT spacing of 44.8 nm, corresponding to a CNT density of 5×10^{10} CNT/cm^2.

within a growing CNT forest increases for the first 100 s of growth,[36,40] indicating that CNTs continually nucleate and grow within the initial stages of CNT forest growth and self-assembly. The current CNT forest growth time of 30 s is well within this regime of increasing nucleation and growth density, and the existence of short, newly nucleated CNTs could be explained by the previous SAXS measurements. An alternative explanation for the short CNTs would be that these CNTs represent CNT fragments of longer CNTs that were well anchored to the substrate and fractured due to high tensile stress; however, the loads provided in the delamination experiments were well below the yield strength of CNTs, as discussed in more detail later.

Further analysis of the substrate delamination region was conducted to estimate the areal density of pits, CNTs, and inactive catalyst particles. Each was counted manually using ImageJ software.[41] Example images may be found in the Supporting Information in which the pits, CNTs, and inactive catalyst particles were counted and identified within the image shown in Figure 3a. Based on this analysis, the approximated areal density of pits was 1.37×10^8/cm^2, the density of unreacted nanoparticles was 1.01×10^8/cm^2, and the density of CNTs was 2.26×10^{10}/cm^2. While the manual SEM counting provides an order of magnitude estimate rather than a precise measurement, these results are in qualitative agreement with SAXS measurements that suggest an increasing number of the CNTs activate during the early stages of CNT forest growth and self-assembly.

Based on the average pillar delamination stress of 6.1 MPa, the approximate adhesion strength for individual CNTs was estimated. An average delamination force of 12.2 nN/CNT was obtained by dividing the delamination stress by the representative CNT areal density of 5×10^{10} CNT/cm^2. Even if the tensile load is assumed to be evenly distributed among CNTs, the tensile stress imparted to each catalyst particle will vary based on the distributed cross-sectional area of each CNT. An estimation of the average CNT adhesion strength was conducted by considering the average CNT delamination force (12.2 nN), and the distributed cross-sectional area provided by CNTs within the population. The adhesion strength was defined relative to the cylindrical CNT cross-sectional area because the contact area between catalyst particles and the substrate may be ill-defined and because the stress carried by CNTs at loss of adhesion may be directly compared between different reports. The numerical calculation used a Monte Carlo method to select CNT diameters from within the log-normal diameter distribution for a population of 1×10^6 CNTs. The inner diameter of each CNT was set as 65% of the outer diameter. The Monte Carlo simulation was run for 100 distinct realizations. The mean adhesion stress was computed using the equation

$$\sigma_m = \frac{1}{N}\sum_{i=1}^{N}\frac{F_d}{A_{c,i}} \quad (1)$$

where σ_m is the mean adhesion strength, N is the number of CNTs (1×10^6), F_d is the average delamination force (12.2 nN), and $A_{c,i}$ is the cross-sectional area of each CNT sampled. This estimation method produced a mean adhesion stress of 269 MPa and a standard deviation of 0.35 MPa.

To better understand how the nonuniform load sharing and complex CNT forest morphology influenced the experimentally measured delamination force of a CNT forest pillar, a finite element mechanical simulation was employed. Briefly, nominally 100 μm tall CNT forests were synthesized in silico using a 2D finite element simulation.[42−44] The simulation span was 30 μm to replicate the diameter of a representative CNT forest pillar shown in Figure 1. A total of 670 CNTs were contained within the simulation domain, corresponding to an average CNT−CNT spacing of 44.8 nm (consistent with a CNT density of 5×10^{10} CNT/cm^2). The outer diameters of the CNTs were assigned based on a log−normal cumulative density function in which the mode was 10 nm. The simulated growth of CNT forests assumed a Gaussian population growth rate distribution characterized by a mean of 60 nm/step and a standard deviation of 3 nm/step. A total of 1500 simulated growth steps were employed to achieve a CNT forest height on the order of 100 μm.

After the simulated CNT synthesis, tensile displacement was applied to the top surface of the simulated forest. To replicate the encapsulation of the top surface in a rigid epoxy, all CNT nodes within 2 μm of the top surface were assumed to be rigidly affixed to a surface that translated vertically at 1−2 nm per time step. The cumulative load was computed at each time step by summing the vertical component of force acting on each node within the simulated epoxy. Each CNT node residing at the growth substrate was assigned an identical adhesion strength, with separate simulations considering adhesion strengths of 200, 300, and 400 MPa. If the stress at the interface exceeded the adhesion strength, the CNT was removed from the substrate.

A representative curve of the simulated tensile force versus displacement is shown in Figure 4a for a CNT forest having a substrate adhesion strength of 400 MPa for each CNT. The

DOI: 10.1021/acsami.9b09979
ACS Appl. Mater. Interfaces 2019, 11, 35221−35227

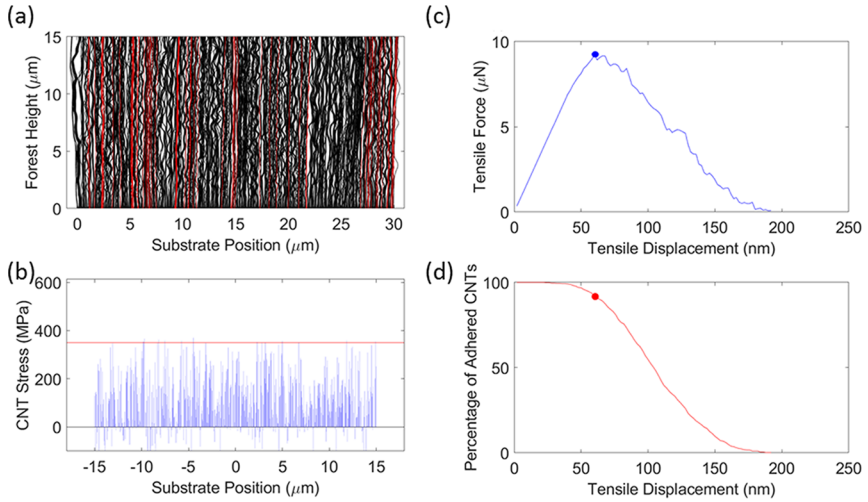

Figure 5. The simulated delamination of CNT forest (670 CNTs on 30 μm substrate). (a) The CNT morphology shown at the maximum observed tensile load at 60 nm displacement. Black CNTs depict adhered CNTs and red CNTs depict delaminated CNTs. (b) A bar chart shows the stress exibited by each CNT at the tensile loading displacement at 64 nm displacement (a). The horizontal red line depicts the CNT adhesion strength of 350 MPa. Plots of (c) the tensile force vs displacement and (d) the percentage of adhered CNTs vs displacement indicate that some CNTs delaminate prior to maximum tensile loading. Note that the circular dot in (c) and (d) correspond to the loading conditions presented in (a). A time-resolved video of this simulation may be found in the Supporting Information.

loading slope initially increases linearly with displacement before reaching a maximum and rapidly decreasing. The decrease in slope can be directly correlated to a decrease in the number of adhered CNTs, as also shown in Figure 4a. The peak load of approximately 8.7 μN, denoted as the CNT forest delamination force, is achieved at approximately 65 nm displacement, followed by a decrease in force and quantity of adhered CNTs. The CNT forest completely delaminated at 200 nm displacement, denoted by both zero force and zero adhered CNTs.

Simulations were conducted using five distinct CNT forests grown from different stochastic parameter selections. The delamination simulations examined uniform CNT adhesion strengths of 200, 300, and 400 MPa, with resulting CNT forest delamination forces shown in Figure 4b. Note that horizontal line at 8.17 μN in Figure 4b represents the cumulative load required to match the experimentally obtained average delamination force of 12.2 nN/CNT. Based on simulations, the experimental CNT delamination force corresponds with a CNT adhesion strength of approximately 350 MPa (Figure 4b). This CNT adhesion strength exceeds the Monte Carlo-based estimation of 269 MPa, likely because the finite element simulation explicitly considers nonuniform load distribution and the progressive loss of CNT adhesion. Note that the adhesion strength is significantly less than the yield strength of multiwalled CNTs (11−63 GPa), indicating that CNTs observed on the catalyst pad after delamination experiments were likely short CNTs rather than fractured CNT segments.

The tensile displacement at which each CNT delaminated was examined relative to the individual CNT length and cross-sectional area. Because each CNT was assigned an identical adhesion strength, it may be anticipated that small-diameter CNTs would experience higher strain and thus lose adhesion first. Surprisingly, no correlation between delamination initiation and CNT diameter was found. Rather, a positive trend between CNT length and the delamination was observed. A plot of CNT delamination as a function of CNT length and tensile displacement is shown in Figure 4c. The linear trend line shows that CNT delamination progresses from the shortest to longest CNTs within the population. The shortest CNTs in the forest are typically vertically oriented, with little excess waviness to accommodate tensile loading. Longer CNTs can accommodate tensile strain by straightening, whereas shorter CNTs directly transmit the load to the substrate. These results indicate that short CNTs disproportionately carry tensile force to the substrate during initial displacement and serve as initiation sites for delamination. The trend of relatively straight CNTs delaminating before wavy CNTs may be seen qualitatively in Figure 5 and a time-sequenced video provided in the Supporting Information.

The stress distribution at the base of the CNT forest was highly nonuniform throughout the tensile loading cycle because of natural variations in CNT tortuosity, length, and diameter. A representative progression of CNT morphology and interfacial stress generated by each CNT during a delamination simulation is shown in Figure 5a,b. The CNT adhesion strength was 350 MPa in the simulation depicted in Figure 5, indicated by a horizontal line in Figure 5b. CNTs with tensile stress that exceeded the adhesion strength were removed from the substrate in the subsequent time step. A fraction of the CNT population experienced a compressive (negative) stress during the initial stages of tensile testing, likely resulting from localized CNT−CNT interactions. On average, the tensile stress increases with increasing tensile displacement. Figure 5b represents a tensile displacement of 64 nm, just past the peak loading of 8.7 μN for this simulation. Note that delamination occurred within the center of the forest rather than at the edges (Figure 5a).

A direct comparison of these results with previous results is difficult because of the disparate nature of previous measurement techniques, adhesion metrics, and synthesis parameters. Perhaps the most direct comparison may be made to direct pull-off techniques in which CNT forests were removed from SiC fibers using adhesive tape. As discussed previously, a delamination stress of 0.28 MPa was observed by others for as-grown CNT forests when using adhesive tape, increasing to 0.5 MPa after annealing at 950 °C in Ar.[15] By considering the reported CNT areal density (1.2×10^{10} CNT/cm^2) and

DOI: 10.1021/acsami.9b09979
ACS Appl. Mater. Interfaces 2019, 11, 35221−35227

average CNT diameter (30 nm, o.d; 10 nm, i.d.), an adhesion strength of 3.7−6.6 MPa (per CNT) is estimated, nearly two orders of magnitude less than the value of 350 MPa reported here. Therefore, the approximately 4-fold increase in CNT density for the current experiments do not account for the enhanced delamination stress observed in the current results. We note that loading in the previous report was likely dominated by shear and that CNT synthesis was achieved by floating catalyst CVD using xylene and ferrocene precursors. Further, the CNT growth mechanism (base-growth vs tip-growth) for the previous report is unclear. Nevertheless, we propose that the drastic increase in CNT delamination strength in this report is not induced by an increase in CNT density but by the catalyst−substrate interaction between iron and aluminum oxide.

By identifying the catalyst−substrate interface as the location of interfacial debonding for our catalyst and synthesis parameters, potential avenues to engineer interfacial adhesion strength may be explored. Qualitatively, we suggest that methods to increase the bonding and interaction between catalyst particles and a substrate or buffer layer are direct routes for increasing the CNT forest delamination strength. Previous reports that utilized annealing steps[15,17] to promote subsurface diffusion of catalyst particles appear to validate this suggestion. Further exploration of bond energies between catalyst particles and substrate materials using atomistic simulation may also identify new buffer layers to promote superior adhesion.

4. CONCLUSIONS

We propose that the in situ uniaxial delamination test methodology and subsequent examination of the delamination surface represents a robust and easily interpreted experimental technique that can help advance the study of interfacial mechanics of CNT forests and similar material systems. Using this approach, an average uniaxial delamination stress of 6.1 MPa was measured for CNT forest micropillars comprised of a relatively high CNT areal density (5×10^{10} CNT/cm^2). Inspection of the substrate and CNT forest after delamination showed that debonding occurred at the interface between the catalyst particles and the substrate rather than at the interface between the CNTs and the catalysts. While the increased CNT density likely contributed to an enhanced delamination stress compared to previous reports, we demonstrate that the increased density is vastly insufficient to account for the increased adhesion per CNT. Delamination simulations show that the entangled and wavy morphology of the CNT forests generated nonuniform load sharing within the CNT population. Consequently, the simulation suggests that the actual adhesion strength of individual CNTs to the growth substrate was approximately 350 MPa. These findings provide new insights into the magnitude of CNT−substrate adhesion, nonuniformity of substrate loading during uniaxial delamination experiments, and identification of the catalyst−substrate interface as the site for CNT forest debonding. Increasing the strength of the catalyst−substrate interaction is expected to enhance the bonding of CNT forests for applications.

■ ASSOCIATED CONTENT

Supporting Information

The Supporting Information is available free of charge on the ACS Publications website at DOI: 10.1021/acsami.9b09979.

Counting of features remaining on a delaminated CNT forest substrate; log−normal CNT diameter probability density function (PDF)

Time-resolved video of CNT forest delamination, including instantaneous CNT stress, tensile force vs tensile displacement, and percentage of adhered CNTs vs tensile displacement (AVI)

■ AUTHOR INFORMATION

Corresponding Author

*E-mail: maschmannm@missouri.edu.

ORCID

Josef Brown: 0000-0002-6225-2065
Taher Hajilounezhad: 0000-0002-8688-8148
Nicholas T. Dee: 0000-0002-8633-3564
Sanha Kim: 0000-0002-3548-6173
A. John Hart: 0000-0002-7372-3512
Matthew R. Maschmann: 0000-0002-0740-6228

Notes

The authors declare no competing financial interest.

■ ACKNOWLEDGMENTS

The authors acknowledge funding from the National Science Foundation (NSF) under award CMMI-1651538, the Air Force Office of Scientific Research (AFOSR) under award FA9550-16-1-0011, and the National Aeronautics and Space Administration (NASA) Space Technology Research Institute (STRI) for Ultra-Strong Composites by Computational Design (US-COMP) grant number NNX17AJ32G.

■ REFERENCES

(1) Arcila-Velez, M. R.; Zhu, J.; Childress, A.; Karakaya, M.; Podila, R.; Rao, A. M.; Roberts, M. E. Roll-to-Roll Synthesis of Vertically Aligned Carbon Nanotube Electrodes for Electrical Double Layer Capacitors. *Nano Energy* **2014**, *8*, 9−16.

(2) Xu, J.; Fisher, T. S. Enhancement of Thermal Interface Materials with Carbon Nanotube Arrays. *Int. J. Heat Mass Transfer* **2006**, *49*, 1658−1666.

(3) Cola, B. A.; Xu, J.; Cheng, C.; Xu, X.; Fisher, T. S.; Hu, H. Photoacoustic Characterization of Carbon Nanotube Array Thermal Interfaces. *J. Appl. Phys.* **2007**, *101*, No. 054313.

(4) Maschmann, M. R.; Dickinson, B.; Ehlert, G. J.; Baur, J. W. Force Sensitive Carbon Nanotube Arrays for Biologically Inspired Airflow Sensing. *Smart Mater. Struct.* **2012**, *21*, No. 094024.

(5) Maschmann, M. R.; Ehlert, G. J.; Dickinson, B. T.; Phillips, D. M.; Ray, C. W.; Reich, G. W.; Baur, J. W. Bioinspired Carbon Nanotube Fuzzy Fiber Hair Sensor for Air-Flow Detection. *Adv. Mater.* **2014**, *26*, 3230−3234.

(6) Nihei, M.; Kawabata, A.; Kondo, D.; Horibe, M.; Sato, S.; Awano, Y. Electrical Properties of Carbon Nanotube Bundles for Future Via Interconnects. *Jpn. J. Appl. Phys.* **2005**, *44*, 1626.

(7) Park, M.; Cola, B. A.; Siegmund, T.; Xu, J.; Maschmann, M. R.; Fisher, T. S.; Kim, H. Effects of a Carbon Nanotube Layer on Electrical Contact Resistance between Copper Substrates. *Nanotechnology* **2006**, *17*, 2294−2303.

(8) de Villoria, R. G.; Hallander, P.; Ydrefors, L.; Nordin, P.; Wardle, B. L. In-Plane Strength Enhancement of Laminated Composites Via Aligned Carbon Nanotube Interlaminar Reinforcement. *Compos. Sci. Technol.* **2016**, *133*, 33−39.

(9) Cebeci, H.; de Villoria, R. G.; Hart, A. J.; Wardle, B. L. Multifunctional Properties of High Volume Fraction Aligned Carbon Nanotube Polymer Composites with Controlled Morphology. *Compos. Sci. Technol.* **2009**, *69*, 2649−2656.

DOI: 10.1021/acsami.9b09979
ACS Appl. Mater. Interfaces 2019, 11, 35221−35227

(10) Wicks, S. S.; de Villoria, R. G.; Wardle, B. L. Interlaminar and Intralaminar Reinforcement of Composite Laminates with Aligned Carbon Nanotubes. *Compos. Sci. Technol.* **2010**, *70*, 20−28.
(11) Qu, L.; Dai, L. Gecko-Foot-Mimetic Aligned Single-Walled Carbon Nanotube Dry Adhesives with Unique Electrical and Thermal Properties. *Adv. Mater.* **2007**, *19*, 3844−3849.
(12) Qu, L.; Dai, L.; Stone, M.; Xia, Z.; Wang, Z. L. Carbon Nanotube Arrays with Strong Shear Binding-on and Easy Normal Lifting-Off. *Science* **2008**, *322*, 238−242.
(13) Lahiri, I.; Lahiri, D.; Jin, S.; Agarwal, A.; Choi, W. Carbon Nanotubes: How Strong Is Their Bond with the Substrate? *ACS Nano* **2011**, *5*, 780−787.
(14) Roumeli, E.; Diamantopoulou, M.; Serra-Garcia, M.; Johanns, P.; Parcianello, G.; Daraio, C. Characterization of Vertically Aligned Carbon Nanotube Forests Grown on Stainless Steel Surfaces. *Nanomaterials* **2019**, *9*, 444.
(15) Cao, A.; Veedu, V. P.; Li, X.; Yao, Z.; Ghasemi-Nejhad, M. N.; Ajayan, P. M. Multifunctional Brushes Made from Carbon Nanotubes. *Nat. Mater.* **2005**, *4*, 540−545.
(16) Pour Shahid Saeed Abadi, P.; Hutchens, S. B.; Greer, J. R.; Cola, B. A.; Graham, S. Buckling-Driven Delamination of Carbon Nanotube Forests. *Appl. Phys. Lett.* **2013**, *102*, 223103.
(17) Su, H.-C.; Chen, C.-H.; Chen, Y.-C.; Yao, D.-J.; Chen, H.; Chang, Y.-C.; Yew, T.-R. Improving the Adhesion of Carbon Nanotubes to a Substrate Using Microwave Treatment. *Carbon* **2010**, *48*, 805−812.
(18) Ageev, O. A.; Blinov, Y. F.; Il'ina, M. V.; Il'in, O.; Smirnov, V. A.; Tsukanova, O. G. Study of Adhesion of Vertically Aligned Carbon Nanotubes to a Substrate by Atomic-Force Microscopy. *Phys. Solid State* **2016**, *58*, 309−314.
(19) Maschmann, M. R.; Zhang, Q.; Wheeler, R.; Du, F.; Dai, L.; Baur, J. In Situ Sem Observation of Column-Like and Foam-Like Cnt Array Nanoindentation. *ACS Appl. Mater. Interfaces* **2011**, *3*, 648−653.
(20) Maschmann, M. R.; Ehlert, G. J.; Park, S. J.; Mollenhauer, D.; Maruyama, B.; Hart, A. J.; Baur, J. W. Visualizing Strain Evolution and Coordinated Buckling within Cnt Arrays by in Situ Digital Image Correlation. *Adv. Funct. Mater.* **2012**, *22*, 4686−4695.
(21) Chen, B.; Goldberg Oppenheimer, P.; Shean, T. A. V.; Wirth, C. T.; Hofmann, S.; Robertson, J. Adhesive Properties of Gecko-Inspired Mimetic Via Micropatterned Carbon Nanotube Forests. *J. Phys. Chem. C* **2012**, *116*, 20047−20053.
(22) Tsai, T. Y.; Lee, C. Y.; Tai, N. H.; Tuan, W. H. Transfer of Patterned Vertically Aligned Carbon Nanotubes onto Plastic Substrates for Flexible Electronics and Field Emission Devices. *Appl. Phys. Lett.* **2009**, *95*, No. 013107.
(23) Pint, C. L.; Xu, Y.-Q.; Moghazy, S.; Cherukuri, T.; Alvarez, N. T.; Haroz, E. H.; Mahzooni, S.; Doorn, S. K.; Kono, J.; Pasquali, M.; Hauge, R. H. Dry Contact Transfer Printing of Aligned Carbon Nanotube Patterns and Characterization of Their Optical Properties for Diameter Distribution and Alignment. *ACS Nano* **2010**, *4*, 1131−1145.
(24) Kumar, A.; Pushparaj, V. L.; Kar, S.; Nalamasu, O.; Ajayan, P. M.; Baskaran, R. Contact Transfer of Aligned Carbon Nanotube Arrays onto Conducting Substrates. *Appl. Phys. Lett.* **2006**, *89*, 163120.
(25) Kim, M. J.; Nicholas, N.; Kittrell, C.; Haroz, E.; Shan, H.; Wainerdi, T. J.; Lee, S.; Schmidt, H. K.; Smalley, R. E.; Hauge, R. H. Efficient Transfer of a Va-Swnt Film by a Flip-over Technique. *J. Am. Chem. Soc.* **2006**, *128*, 9312−9313.
(26) Pint, C. L.; Xu, Y.-Q.; Pasquali, M.; Hauge, R. H. Formation of Highly Dense Aligned Ribbons and Transparent Films of Single-Walled Carbon Nanotubes Directly from Carpets. *ACS Nano* **2008**, *2*, 1871−1878.
(27) Murakami, Y.; Maruyama, S. Detachment of Vertically Aligned Single-Walled Carbon Nanotube Films from Substrates and Their Re-Attachment to Arbitrary Surfaces. *Chem. Phys. Lett.* **2006**, *422*, 575−580.
(28) Huang, J.-Q.; Zhang, Q.; Zhao, M.-Q.; Wei, F. The Release of Free Standing Vertically-Aligned Carbon Nanotube Arrays from a Substrate Using Co2 Oxidation. *Carbon* **2010**, *48*, 1441−1450.
(29) Yang, X.; Yuan, L.; Peterson, V. K.; Minett, A. I.; Yin, Y.; Harris, A. T. Facile Preparation of Free-Standing Carbon Nanotube Arrays Produced Using Two-Step Floating-Ferrocene Chemical Vapor Deposition. *ACS Appl. Mater. Interfaces* **2012**, *4*, 1417−1422.
(30) Wang, M.; Li, T.; Yao, Y.; Lu, H.; Li, Q.; Chen, M.; Li, Q. Wafer-Scale Transfer of Vertically Aligned Carbon Nanotube Arrays. *J. Am. Chem. Soc.* **2014**, *136*, 18156−18162.
(31) Zhang, M.; Atkinson, K. R.; Baughman, R. H. Multifunctional Carbon Nanotube Yarns by Downsizing an Ancient Technology. *Science* **2004**, *306*, 1358−1361.
(32) Brieland-Shoultz, A.; Tawfick, S.; Park, S. J.; Bedewy, M.; Maschmann, M. R.; Baur, J. W.; Hart, A. J. Scaling the Stiffness, Strength, and Toughness of Ceramic-Coated Nanotube Foams into the Structural Regime. *Adv. Funct. Mater.* **2014**, *24*, 5728−5735.
(33) Pour Shahid Saeed Abadi, P.; Maschmann, M. R.; Hodson, S. L.; Fisher, T. S.; Baur, J. W.; Graham, S.; Cola, B. A. Mechanical Behavior of Carbon Nanotube Forests Grown with Plasma Enhanced Chemical Vapor Deposition: Pristine and Conformally Coated. *J. Eng. Mater. Technol.* **2017**, *139*, No. 034502.
(34) Hutchens, S. B.; Hall, L. J.; Greer, J. R. In Situ Mechanical Testing Reveals Periodic Buckle Nucleation and Propagation in Carbon Nanotube Bundles. *Adv. Funct. Mater.* **2010**, *20*, 2338−2346.
(35) Pathak, S.; Lim, E. J.; Pour Shahid Saeed Abadi, P.; Graham, S.; Cola, B. A.; Greer, J. R. Higher Recovery and Better Energy Dissipation at Faster Strain Rates in Carbon Nanotube Bundles: Anin-SituStudy. *ACS Nano* **2012**, *6*, 2189−2197.
(36) Bedewy, M.; Hart, A. J. Mechanical Coupling Limits the Density and Quality of Self-Organized Carbon Nanotube Growth. *Nanoscale* **2013**, *5*, 2928−2937.
(37) Dee, N. T.; Li, J.; White, A. O.; Jacob, C.; Shi, W.; Kidambi, P. R.; Cui, K.; Zakharov, D. N.; Janković, N. Z.; Bedewy, M.; Chazot, C. A. C.; Carpena-Núñez, J.; Maruyama, B.; Stach, E. A.; Plata, D. L.; Hart, A. J. Carbon-Assisted Catalyst Pretreatment Enables Straightforward Synthesis of High-Density Carbon Nanotube Forests. *Carbon* **2019**, *153*, 196−205.
(38) Bedewy, M.; Viswanath, B.; Meshot, E. R.; Zakharov, D. N.; Stach, E. A.; Hart, A. J. Measurement of the Dewetting, Nucleation, and Deactivation Kinetics of Carbon Nanotube Population Growth by Environmental Transmission Electron Microscopy. *Chem. Mater.* **2016**, *28*, 3804−3813.
(39) Carpena-Núñez, J.; Boscoboinik, J. A.; Saber, S.; Rao, R.; Zhong, J.-Q.; Maschmann, M. R.; Kidambi, P. R.; Dee, N. T.; Zakharov, D. N.; Hart, A. J.; Stach, E. A.; Maruyama, B. Isolating the Roles of Hydrogen Exposure and Trace Carbon Contamination on the Formation of Active Catalyst Populations for Carbon Nanotube Growth. *ACS Nano* **2019**, 8736.
(40) Bedewy, M.; Meshot, E. R.; Reinker, M. J.; Hart, A. J. Population Growth Dynamics of Carbon Nanotubes. *ACS Nano* **2011**, *5*, 8974−8989.
(41) Rueden, C. T.; Schindelin, J.; Hiner, M. C.; DeZonia, B. E.; Walter, A. E.; Arena, E. T.; Eliceiri, K. W. Imagej2: Imagej for the Next Generation of Scientific Image Data. *BMC Bioinf.* **2017**, *18*, 529.
(42) Maschmann, M. R. Integrated Simulation of Active Carbon Nanotube Forest Growth and Mechanical Compression. *Carbon* **2015**, *86*, 26−37.
(43) Hajilounezhad, T.; Ajiboye, D. M.; Maschmann, M. R. Evaluating the Forces Generated During Carbon Nanotube Forest Growth and Self-Assembly. *Materialia* **2019**, *7*, 100371.
(44) Hajilounezhad, T.; Maschmann, M. R. Numerical Investigation of Internal Forces During Carbon Nanotube Forest Self-Assembly. In *ASME 2018 International Mechanical Engineering Congress and Exposition*; American Society of Mechanical Engineers Digital Collection: 2018 (52019) V002T02A088.

DOI: 10.1021/acsami.9b09979
ACS Appl. Mater. Interfaces 2019, 11, 35221−35227